Amorphous to amorphous insulator-metal transition in $GeSe_3$:Ag glasses

Kiran Prasai, Gang Chen, and D. A. Drabold*
Department of Physics and Astronomy, Ohio University, Athens, Ohio 45701, USA
(Received 7 March 2017; published 26 June 2017)

We study an insulator-metal transition in a ternary chalcogenide glass $(GeSe_3)_{1-x}Ag_x$ for $x = 0.15$ and 0.25. The conducting phase of the glass is obtained by using gap sculpting [Prasai *et al.*, Sci. Rep. **5**, 15522 (2015)] and it is observed that the metallic and insulating phases have nearly identical density functional energies but have a conductivity contrast of $\sim 10^8$. As such, we demonstrate an example of polyamorphism for which energetically close phases exhibit dramatically different optical properties. The transition from insulator to metal involves growth of an Ag-rich phase accompanied by a depletion of tetrahedrally bonded $Ge(Se_{1/2})_4$ in the host network. The relative fraction of the amorphous Ag_2Se phase and $GeSe_2$ phase is shown to be a critical determinant of dc conductivity.

DOI: 10.1103/PhysRevMaterials.1.015603

I. INTRODUCTION

Metal-Insulator transitions (MIT) and their associated science are among the cornerstones of condensed matter physics [1]. In this paper, we describe the atomistics of a technically important but poorly understood MIT in GeSe:Ag glasses, a prime workhorse of conducting bridge memory (CBRAM) devices [2,3]. By design, we construct a stable conducting model from a slightly energetically favored insulating phase. Predictions are made for structural, electronic, and transport properties. We demonstrate the utility of our gap sculpting method [4] as a tool of materials design.

We report metallic phases of amorphous $(GeSe_3)_{1-x}Ag_x$ at $x = 0.15$ and 0.25. These are canonical examples of Ag-doped chalcogenide glasses, which are studied in relation to their photoresponse and diverse optoelectronic applications [5,6]. Ag is remarkably mobile making the material a solid electrolyte and is known to act as "network modifier" in these glasses as it alters the connectivity of network. Experiments have shown Se-rich ternaries $[(Ge_ySe_{1-y})_{1-x}Ag_x$ with $y < 1/3]$ to be phase-separated into an Ag-rich Ag_2Se phase and a residual Ge_tSe_{1-t} phase [7].

Using first-principles calculations, we show that stable amorphous phases with at least $\sim 10^8$ times higher electronic conductivity exist with only a small ($\approx$0.04 eV/atom) difference in total energy. These conducting states present the same basic structural order in the glass, but have a higher relative fraction of an a-Ag_2Se phase compared to the insulating states. It is known that amorphous materials are characterized by large numbers of degenerate conformations that are mutually accessible to each other at small energy cost, but those usually have similar macroscopic properties. The remarkable utility of these materials accrues from states with distinct properties, nevertheless readily accessible to each other.

We discover the conducting phase of $GeSe_3Ag$ glass by *designing* atomistic models with a large density of states (DOS) near the Fermi energy [4]. This is achieved by utilizing Hellmann-Feynman forces from the band edge states. These forces are used to bias the true forces in *ab initio* molecular dynamics (AIMD) simulations to form structures with a large DOS at the Fermi level. The biased force on atom α, $F_\alpha^{\rm bias}$, is obtained by suitably summing Hellmann-Feynman forces for the band edge states [second term in Eq. (1)] with the total force from AIMD calculations, $F_\alpha^{\rm AIMD}$,

$$F_\alpha^{\rm bias} = F_\alpha^{\rm AIMD} + \sum_i \gamma_i \langle \psi_i | \frac{\partial H}{\partial R_\alpha} | \psi_i \rangle. \quad (1)$$

Here, γ's set the sign and magnitude of the HF forces from individual states i. To maximize the density of states near ϵ_F, gap states closer to the valence edge will have $\gamma > 0$, whereas the states in the conduction edge will have $\gamma < 0$. The magnitude of γ determines the size of biasing force (with $\gamma = 0$ representing true AIMD forces). We have employed biased forces as an electronic constraint to model semiconductors and insulators in our recently published work [8] where the biasing is done in just the opposite sense: to force states out of the band gap region.

II. COMPUTATIONAL APPROACH

We start with conventional 240 atom models of $(GeSe_3)_{1-x}Ag_x$, $x = 0.15$ and 0.25, at their experimental densities 5.03 and 5.31 gm cm^{-3} [9], respectively. These were prepared using melt-quench MD simulations, followed by conjugate-gradient relaxation to a local energy minimum. The MD simulations are performed using the Vienna *ab initio* simulation package (VASP) [10]. Plane waves of up to 350 eV are used as basis and DFT exchange correlation functionals of Perdew-Burke-Ernzerhof [11] were used. Brillouin zone (BZ) is represented by Γ point for bulk of the calculations. For static calculations, BZ is sampled over 4 k points. These models fit the experimental structure factor reasonably well (Fig. 1).

We obtain conducting conformations by annealing the starting configurations using biased forces at 700 K for 18 ps. The electronic states in the energy range $[\epsilon_F - 0.4\,\text{eV}, \epsilon_F + 0.4\,\text{eV}]$ are included in the computation of bias force and $|\gamma_i| = 3.0$ is used. The bias potential $[\Phi_b(R_1, \ldots, R_{3N}) = \sum -\gamma_i \langle \psi_i | H(R_1, \ldots, R_{3N}) | \psi_i \rangle]$ shepherds the electronic states at the band edges into the band-gap region. Since we want any proposed metallic conformation to be a minimum of the unbiased DFT energy functional, we relax instantaneous snapshots of biased dynamics (taken at the interval of 0.2 ps,

*drabold@ohio.edu

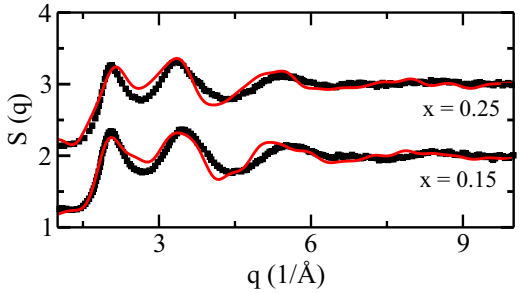

FIG. 1. The structure factor of $(GeSe_3)_{1-x}Ag_x$ models (solid red line) compared with experiment (black squares) [9].

leaving out the first 4 ps) to their nearest minima using conjugate gradient algorithm with true DFT-GGA forces. We study all relaxed snapshots by (i) gauging the density and localization of states around the Fermi energy and (ii) testing the stability of the configurations by annealing them at 300 K (N.B. glass transition temperatures (T_g) are 488 and 496 K for compositions $x = 0.15$ and 0.25 respectively [12]). At each composition, we selected five models that display a large density of extended states around Fermi energy and are stable against extended annealing at 300 K as the "metallized" models. These metallized systems are, on average, 0.040 ± 0.009 eV per atom above their insulating counterparts.

III. RESULTS

A. Electronic structure and transport

The metallized models, by construction, exhibit a large density of states around the Fermi energy (Fig. 2) whereas the insulating models display a small but well defined PBE gap of 0.41 and 0.54 eV for $x = 0.15$ and 0.25, respectively. For disordered materials, a high DOS at ϵ_F *alone* may not produce conducting behavior since these states can be localized (example: amorphous graphene [13]). We gauge the localization of these states by computing inverse participation ratio (IPR [14]) (plotted for $x = 0.25$ system in Fig. 3) and show that these states *are* indeed extended. We compute the electronic conductivity $[\sigma(\omega)]$ using the Kubo-Greenwood formula (KGF) in the following form:

$$\sigma_k(\omega) = \frac{2\pi e^2\hbar^2}{3m^2\omega\Omega}\sum_{j=1}^{N}\sum_{i=1}^{N}\sum_{\alpha=1}^{3}[F(\epsilon_i,k) - F(\epsilon_j,k)] \times |\langle\psi_{j,k}|\,\nabla_\alpha\,|\psi_{i,k}\rangle|^2\delta(\epsilon_{j,k} - \epsilon_{i,k} - \hbar\omega) \quad (2)$$

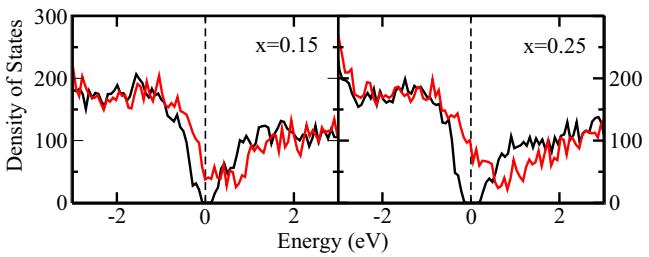

FIG. 2. The electronic density of states (DOS) of the insulating model (black curve) and the metallized model (red curve). Energy axis is shifted to have Fermi level at 0 eV (the broken vertical line).

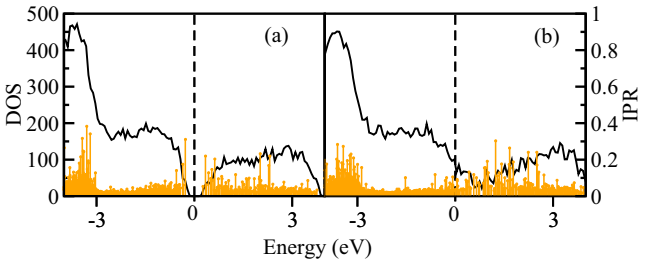

FIG. 3. The (black curve) electronic density of states (DOS) and (orange drop lines) Inverse Participation Ratio (IPR) of the insulating model (a) and the metallized model (b). The energy axis for all data sets is shifted to have Fermi level at 0 eV (highlighted by the broken vertical line).

It has been used with reasonable success to predict conductivity [15]. Our calculations used 4 k points to sample the Brillouin zone. To compensate for the sparseness in the DOS due to the size of the supercell, a Gaussian broadening (δE) for the δ function is used. We note that the choice of δE between 0.01 and 0.1 eV does not significantly alter the computed values of DC conductivity $[\sigma(\omega = 0)]$ (Fig. 4). For the choice of $\delta E = 0.05$ eV (which is small compared to the thermal fluctuation of Kohn-Sham states for disordered systems at room temperature. For a heuristic theory, see [16]), the dc conductivity of metallic models are of the order of $10^2\ \Omega^{-1}\,cm^{-1}$ at both concentrations. For the insulating model at $x = 0.15$, this value is of order $10^{-6}\ \Omega^{-1}\,cm^{-1}$ whereas for insulating model at $x = 0.25$, this value is lower but can not be ascertained from our calculations. We find that the metallized models show, at least, $\sim 10^8$ times higher conductivity than the insulating models. The computed conductivity for metallic models are comparable to the dc conductivity values of liquid silicon ($\approx 10^4\ \Omega^{-1}\,cm^{-1}$ [17]).

B. Structure of conducting phase

We track the atomic rearrangements associated with the metallization of the network to identify the microscopic origin of metallicity. Recalling that these are inhomogenous glasses with phase separation into an Ag-rich a-Ag_2Se phase and a

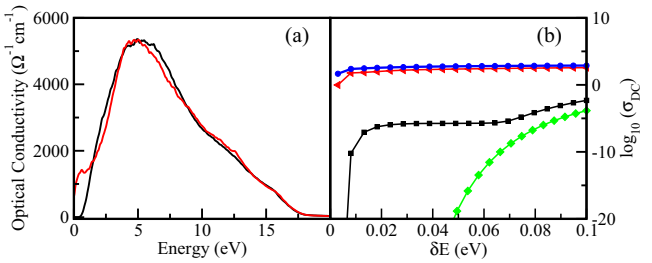

FIG. 4. (a) Optical conductivity of insulating (black curve) and metallized (red curve) models for $(GeSe_3)_{0.75}Ag_{0.25}$ model computed using Kubo-Greenwood formula. Brillouin zone sampling is done over four k points and averaged over three directions to eliminate artificial anisotropy. (b) dc conductivity as a function of Gaussian approximant δE (see text). Black squares: insulating model at $x = 015$, red triangles: metallic model at $x = 0.15$, green diamonds: insulating model at $x = 0.25$, blue circles: metallic model at $x = 0.25$.

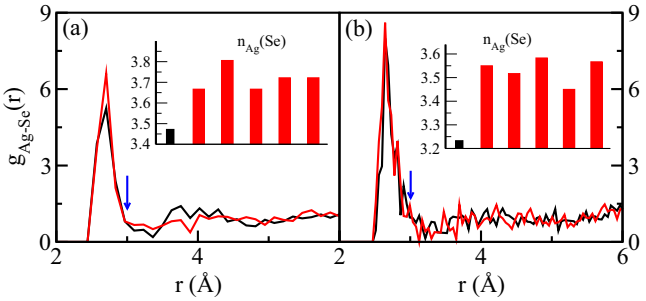

FIG. 5. The Ag-Se correlation in insulating (black) and metallized (red) models at two concentrations of silver (a) $x = 0.15$ and (b) 0.25. The histogram in inset shows the Se coordination around Ag atoms [n_{Ag}(Se)] for insulating (black) and five metallic (red) confirmations at both values of x. The cutoff for computing coordination is 3.00 Å, highlighted by an arrow.

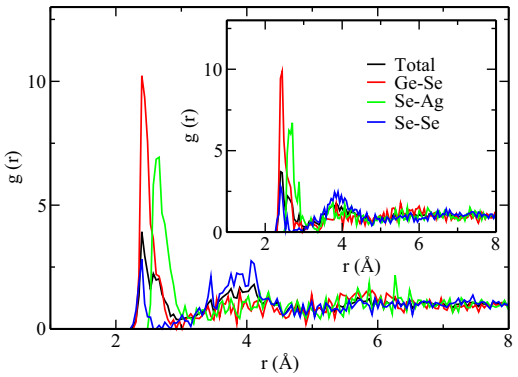

FIG. 7. The partial pair correlation functions of the metallized models at $x = 0.15$. Inset presents these correlation functions for insulating models. The remaining Ge-Ge, Ag-Ag, and Ge-Ag correlations are noisy and are not presented here.

residual Ge-Se backbone, we note that the insulator-metal transition in these glasses can be viewed in terms of the relative ratio of these two competing phases. In particular, we make the following three observations associated with the insulator-metal transition: (i) growth of Ag-Se phase, (ii) depletion of tetrahedral $GeSe_2$ phase, and (iii) growth of Ge-rich phase in the host network. Below we briefly comment on these three observations, a more detailed account of structural rearrangements will be published later.

Growth of Ag-Se phase. We observe that the Ag-Se phase grows upon metallization. Se-Ag correlation ($r_{\text{Ag-Se}} = 2.67$ Å) is found to increase from the insulating to metallic model (see Fig. 5, also the increase in peak P2 in Fig. 6). For both Ag concentrations, Se coordination around Ag is found to increase from insulating to metallic models. For $x = 0.15$, Se coordination around Ag increases from 3.47 to 3.72 (the later value is an average over 5 metallic models, see Fig. 5). For $x = 0.25$, it increases from 3.23 to (on average) 3.53.

Depletion of tetrahedral $GeSe_2$. The network in the insulating phase is dominated by Se-rich tetrahedral $Ge(Se_{1/2})_4$, accompanied by a competing Ag-Se phase. The fraction of the later phase is directly determined by the Ag concentration in the network. These two phases appear as two distinct peaks in the total radial distribution function (RDF) (Figs. 6 and 7). Upon metallization, the growth of Ag-Se shifts the balance of stoichiometries in the network and the host network becomes Se deficient. At composition $x = 0.25$ (plotted in Fig. 6), the network in the metallic phase is dominated by the Ag-Se subnetwork (peak P2). The corresponding Ge-Se coordination number in the metallic model is 3.22, slightly lower than 3.40 in the insulating model. For $x = 0.15$, these values are 3.28 and 3.43, respectively. The correlation cutoff of 2.70 Å is taken to determine the coordinations.

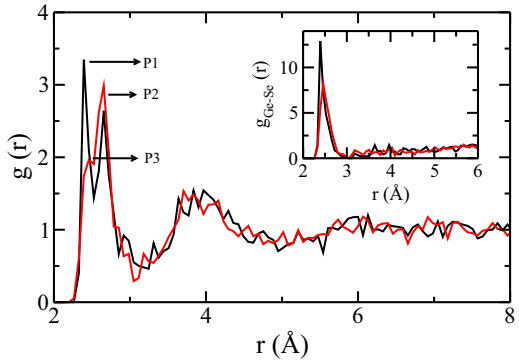

FIG. 6. The total radial distribution function [g(r)] of the insulating and metallized models (black and red curves, respectively) at $x = 0.25$. Note the bifurcated first peak originates from Ge-Se correlation (P1 at 2.40 Å) and Ag-Se correlation (P2 at 2.67 Å). For the metallized model, peak P3 arises due to depletion of tetrahedral $Ge(Se_{1/2})_4$ and formation of Ge-rich Ge-Se phases.

Growth of Ge-rich phase in the host network. The host network of Ge-Se consists of Se-rich tetrahedral $GeSe_2$ and nontetrahedral Ge-rich phases including the ethanelike Ge_2Se_3 units. These subnetworks were reported in $GeSe_2$ by Boolchand and coworkers [18] and in ternary chalcogenide glasses by Mitkova and coworkers [19]. We find that these Ge-Se stoichiometries have different bondlength distributions: Se-rich phases ($n_{\text{Ge-Se}} \geqslant 4$) have bondlengths smaller than 2.55 Å, whereas Ge-rich phases ($n_{\text{Ge-Se}} < 4$) have bondlengths longer than 2.55 Å. In an insulating conformation, the former phase dominates and registers an RDF peak at ≈2.40 Å (Fig. 6). For metallic conformations, fewer Se atoms are available to Ge. This increases the fraction of Ge-rich phases and the Ge-Se bondlength distribution shifts to longer distances. This is represented by a shift in the Ge-Se pair correlation function in Fig. 6 (inset) and the appearance of peak P3 in the total RDF. Due to increase in the fraction of $Ge_2(Se_{1/2})_6$, the Ge-Ge correlation peak appears around 3.5 Å in metallic models. We note that it is such a Ge-Ge signal in Raman scattering and ^{119}Sn Mössbauer spectroscopy that led to the experimental discovery of Ge-rich $Ge_2(Se_{1/2})_6$ phase in stoichiometric bulk Ge_xSe_{100-x} glasses [18].

C. Electronic activity of Ag-Se phase

Now we comment further on the role of the Ag-Se phase in conduction. It is well known that the states around the Fermi energy are mainly Se p orbitals ([20,21], in GeSAg [22]). The electronic structure of the metallic model projected onto its constituent subnetworks (Ag-Se and Ge-Se) shows different

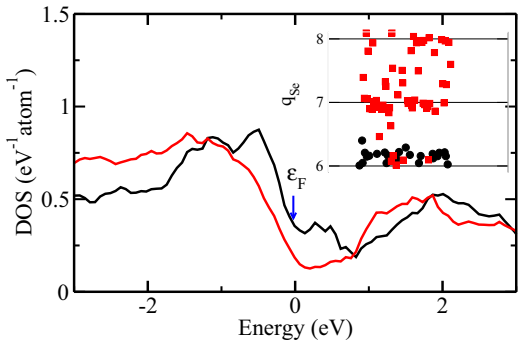

FIG. 8. The density of states of the metallic model projected onto Se atoms in the two subnetworks: Ag-Se subnetwork (black curve) and Ge-Se subnetwork (red curve). Since these two subnetworks contain different numbers of Se atoms (23 and 59 for this plot), an average was taken to enable comparison. Se atoms bonded to both Ge and Ag are not included in the calculation. The energy axis was shifted to have Fermi energy (ϵ_F) at 0 eV. The inset shows Bader charges (q_{Se}) for the same two groups of Se atoms. Black filled circles represent Se in the Ag-Se network, red filled squares represent Se in the Ge-Se network.

electronic activity of Se atoms in the two subnetworks. We find that Se atoms in the Ag_2Se network have twice as much projection around the Fermi energy than the Se atoms in the Ge-Se network (Fig. 8). This suggests that a more concentrated Ag-Se network will enhance the conduction. Experimentally, growth of Ag-rich nanocrystals in a GeS_2 matrix has been shown to enhance the *electronic* conductivity [23]. The Se atoms in the Ag-Se phase are found in the atomic state ($q_{Se} \sim 0$) whereas those in the Ge-Se network are ionic with negative charge ($q_{Se} \sim -1$ or -2) (see inset in Fig. 8).

IV. DISCUSSION

In the more general context of oxides and chalcogenides, the states in the energy gap are associated with oxygen or chalcogen *p* states. An insulator-metal transition thus involves phase separation of a material into an oxygen or chalcogen-rich phase embedded in an oxygen or chalcogen deficit matrix. Such a process has been experimentally and theoretically demonstrated in amorphous gallium oxide [24] wherein a transition to a metallic phase is shown to involve formation of O-rich Ga_2O_3 nanocrystals accompanied by an O-depleted Ga-O matrix. In the case of GeS_2:Ag_2S, it has been reported that the size of Ag_2S nanocrystallites in a GeS_2 matrix correlates directly with the electronic conductivity of the composite sample, and for sufficiently large nanocrystallites, approaches the conductivity of Ag_2S film [23]. The formation of Ag_2S and a Ge-rich host network upon the addition Ag atoms has been observed using Raman spectroscopy [25] and this supports our observation of formation of Ge-rich backbone upon metallization.

The observed conducting phase of $GeSe_3$:Ag does not require Ag wires as often supposed. The conductivity of our phase is still rather low, of order of 200 $\Omega^{-1}\,cm^{-1}$, and due to an impurity band formed at the Fermi level, associated with Se *p* orbitals on certain Se-atoms bonded to Ag atoms. The impurity bands depend on the concentration of Ag and phase separation. More discussion on the conduction through impurity bands and resonant clusters [26] will be published in a separate paper. We note here that the observed weakly conducting phases might correspond to recent observations by Chen and coworkers [27] of intermediate-phase switching in $GeSe_2$:Ag. Such intermediate conducting phase is induced by applying a weak electrochemical bias and is observed before the onset of Ag-nanowire formation.

The metallic and insulating phases reported here are an unusual example of poly-amorphism. It is interesting to observe that amorphous phases that are energetically similar can exhibit markedly different transport behavior.

V. CONCLUSIONS

Altogether, we have presented a direct simulation of the conducting phase of CBRAM material $GeSe_3Ag$ and it provides evidence of the conduction through interconnected regions of the Ag_2Se phase in the glassy matrix [23]. This work does not attempt to describe the conduction through Ag nanowires, which may be the mechanism of conduction in two-terminal metal-electrolyte-metal devices [28]. It demonstrates the existence of metastable amorphous forms ("polyamorphism") of the glass with drastically different optical response. The observation that the DFT energies of these states are only 0.04 eV per atom higher than insulating state suggests that these states might to accessible. We also showed by direct computation that our gap sculpting method can be an effective tool to explore/discover phases of matter with desired optical properties.

ACKNOWLEDGMENTS

We thank M. Mitkova, P. Boolchand, and M. N. Kozicki for stimulating discussions. This work is supported by National Science Foundation under Grant Nos. DMR 1506836, DMR 1507670, and DMR 1507166. We are thankful to the Ohio Supercomputer center for computing resources.

[1] N. F. Mott and E. A. Davis, *Electronic Processes in Non-Crystalline Materials* (OUP Oxford, Oxford, 2012).
[2] M. N. Kozicki and M. Mitkova, U.S. Patent No. 6,635,914 (2003).
[3] I. Valov, R. Waser, J. R. Jameson, and M. N. Kozicki, Nanotechnology **22**, 254003 (2011).
[4] K. Prasai, P. Biswas, and D. A. Drabold, Sci. Rep. **5**, 15522 (2015).
[5] *Photo-Induced Metastability in Amorphous Semiconductors*, edited by A. V. Kolobov (Wiley, Weinheim, 2006).
[6] M. Mitkova, Real Time Optical Recording on Thin Films of Amorphous Semiconductors, in *Insulating and Semiconducting Glasses*, edited by P. Boolchand, Series on Directions in Condensed Matter Physics Vol. 17 (World Scientific, Singapore, 2000).

[7] M. Mitkova, Y. Wang, and P. Boolchand, Phys. Rev. Lett. **83**, 3848 (1999).
[8] K. Prasai, P. Biswas, and D. A. Drabold, Phys. Status Solidi A **213**, 1653 (2016).
[9] A. Piarristeguy, M. Mirandou, M. Fontana, and B. Arcondo, J. Non-Cryst. Solids **273**, 30 (2000).
[10] G. Kresse and J. Furthmüller, Phys. Rev. B **54**, 11169 (1996); Comput. Mater. Sci. **6**, 15 (1996).
[11] J. P. Perdew, K. Burke, and M. Ernzerhof, Phys. Rev. Lett. **77**, 3865 (1996).
[12] B. Arcondo, M. Urena, A. Piarristeguy, A. Pradel, and M. Fontana, Physica B: Condens. Matter **389**, 77 (2007).
[13] D. Van Tuan, A. Kumar, S. Roche, F. Ortmann, M. F. Thorpe, and P. Ordejon, Phys. Rev. B **86**, 121408(R) (2012).
[14] J. M. Ziman, *Models of Disorder: the Theoretical Physics of Homogeneously Disordered systems* (CUP Archive, Cambridge, 1979).
[15] T. A. Abtew, M. Zhang, and D. A. Drabold, Phys. Rev. B **76**, 045212 (2007); G. Galli, R. M. Martin, R. Car, and M. Parrinello, *ibid.* **42**, 7470 (1990); P. B. Allen and J. Q. Broughton, J. Phys. Chem. **91**, 4964 (1987).
[16] K. Prasai, P. Biswas, and D. A. Drabold, Semicond. Sci. Technol. **31**, 073002 (2016).
[17] V. M. Glazov, S. N. Chizhevskaya, and N. N. Glagoleva, *Liquid Semiconductors* (Plenum Press, New York, 1969), p. 362.
[18] P. Boolchand and W. Bresser, Philos. Mag. B **80**, 1757 (2000).
[19] M. Mitkova, M. Kozicki, H. Kim, and T. Alford, J. Non-Cryst. Solids **352**, 1986 (2006).
[20] B. Prasai and D. A. Drabold, Phys. Rev. B **83**, 094202 (2011).
[21] D. N. Tafen, D. A. Drabold, and M. Mitkova, Phys. Rev. B **72**, 054206 (2005).
[22] J. Akola, B. Beuneu, R. Jones, P. Jóvári, I. Kaban, J. Kolář, I. Voleská, and T. Wágner, J. Phys.: Condens. Matter **27**, 485304 (2015).
[23] R. Y. Wang, R. Tangirala, S. Raoux, J. L. Jordan-Sweet, and D. J. Milliron, Adv. Mater. **24**, 99 (2012); R. Waser, R. Dittmann, G. Staikov, and K. Szot, *ibid.* **21**, 2632 (2009).
[24] L. Nagarajan, R. A. De Souza, D. Samuelis, I. Valov, A. Börger, J. Janek, K.-D. Becker, P. C. Schmidt, and M. Martin, Nat. Mater. **7**, 391 (2008).
[25] M. Balakrishnan, M. N. Kozicki, C. D. Poweleit, S. Bhagat, T. L. Alford, and M. Mitkova, J. Non-Cryst. Solids **353**, 1454 (2007).
[26] J. Dong and D. A. Drabold, Phys. Rev. Lett. **80**, 1928 (1998).
[27] G. Chen (private communication).
[28] M. N. Kozicki, M. Mitkova, and I. Valov, Electrochemical Metallization Memories, in *Resistive Switching: From Fundamentals of Nanoionic Redox Processes to Memristive Device Applications*, edited by D. Ielmini and R. Waser (Wiley, Weinheim, 2015), pp. 483–514.